Automated measurement of cylinder volume by vision

G. Deltel, C. Gagné, A. Lemieux, M. Levert, X. Liu, L. Najjar, X. Maldague

Electrical and Computing Engineering Dept (Computing Vision and Systems Laboratory[1])
Université Laval, Quebec (Quebec) Canada G1K 7P4

1. Introduction

In the current application, sample density (= mass / volume [g/cm^3]) of cylindrically shaped objects is measured by first obtaining the sample weight (with a digital scale) and then the volume V which is manually measured using gallipers (for a cylinder of length L and radius R:

$$V = L\,(\pi R^2). \tag{1}$$

In the traditional approach, the operator measures up to three diameters and three lengths at different angles on the specimen. Such density measurement is an important quality criteria for the fabrication process of the involved company. In order to speed up the application and also insure a better reproducibility (manual measurement is always prone to operator's errors), an automatic acquisition of the sample volume was in need. The purpose of this paper is thus to present the method which was designed to acquire the volume. The retained method is based on a a non-contact vision procedure.

Obviously, the vision method has to provide measurements at least as well as accurate as the manual testing, that is to achieve a 0.1 cm^3 for specimens of 50 to 150 mm in length and of 5 cm diameter. Moreover, measurement duration should be in the same range with respect with the manual testing, that is about 1 minute per sample, and preferably less.

2. Measurement principle

Although various vision approaches are possible such as active 3D/laser, defocusing, stereo methods /1, 2/, a simple one camera-back lighting approach was developed. Schematic diagrams and pictures of the system are shown in Fig. 1. The measurement apparatus consists of:
1° fluorescent ring annulus (22 W),
2° diffusing white glass plate,
3° two rotating rods on which the sample is positioned horizontally,
4° gears and stepping motor (1.8°/step) to rotate the rods,
5° camera (512 x 480 pixels) and lens (16 mm),
6° computer (PC) to frame-grab the images, control the stepping motor and perform the volume computations.

1. www.gel.ulaval.ca/~vision

The measurement principle is as follow:

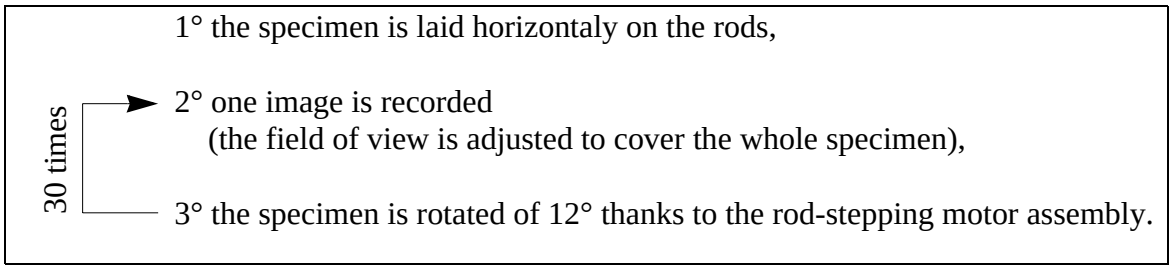

In fact this acquisition methods mimics somehow the traditional method used by the operator manipulating the sample with the gallipers. Advantages of the approach are: simple set-up with limited number of components, non-contact, no gas involved (as in an immersion approach following Archimed principle for which the displaced volume of liquid of an immersed object is equal to the volume of that same object).

Finally, it should be noted that rubber O-rings were added on the rods to prevent any slipping of the objects during the rotation (Fig. 1). Moreover, a delay is added after the motor is stopped to allow mechanical vibrations to vanish before image acquisition (this could be suppress in an enhanced acquisition mechanism).

3. Image processing

The purpose of the image processing is to extract *L* and *R* as in eq. (1). The many images acquired allow to improve accuracy by averaging /1/, all details are available in /2/.

Fig. 2 shows an original image in gray levels. As noticed, the object is well distinguished from the background. Moreover the perspective projection effect is well seen at the extremities of the specimen which are curved (while they are straight for specimens) and this will have to be taken into account. Acquired images are in fact shadow images of the cylinder due to the back lighting involved.

The first processing step consists to binarize the image *I*. This is accomplished as follow. Each original image I_o is first normalized in between 0 and 1 (1 for black). Next gray levels between 0 and 0.5 are set to 0 value (white):

$$
\begin{aligned}
&I_N = norm(I_o), \text{ with:} \\
&norm(x) = \frac{x - min(x)}{max(x) - min(x)} \\
&I_F = cut(I_N, 0.5), \text{ with:} \\
&cut(x, s) = \begin{pmatrix} 0 \text{ for } |x| \le s \\ 0 \text{ for } |x| > s \end{pmatrix}
\end{aligned}
\qquad (2)
$$

in which I_N is the normalized image and I_F the filtered image.Figure 3 shows result of this procedure which allows for a noise reduction in high intensity regions (pixels having a normalized intensity of less than 1). In the next step a classical Sobel /1/ operator is used to extract edges. In fact only vertical edges are extracted in order to compute the diameter of the cylinder. Fig. 4 shows the resulting image. Since the detected edges have a few pixel thickness, they are subse-

quently thinned to the point where the intensity variation are the greatest: first minimum and maximum values in each column of the amplitude matrix (= image of Fig. 4) are found and then an empirically threshold of 2 is applied on the (max-min) difference to locate the positions where the gray level variations are the greatest. Such a procedure is more accurate than a straight threshold applied directly on image of Fig. 2. The result of this procedure is shown on Fig. 5. A first estimation of the diameter is then obtained as the min-max index difference in the image matrix. Negative values are rejected. Moreover, smaller differences correspond to rod locations and are rejected as well as extremity values which are due to the curvature of the perspective projection effect. Averaging allows to improve the diameter values (the signal-to-noise ratio is increased by the square root of the number of averaged images) /1/. Cylinder length is obtained by counting the number of column in the image matrix where diameter are non-null values. We finally obtained, for every image, an average diameter D ($R = D/2$) and length L. Since a sequence of images are available, the volume is computed with eq. (1) for every image and then an median-average is computed. The median-average consists in averaging together 80% of the statistically central volume values.

Previous computations provide results in pixels and volume in pixel^3. A calibration process is next required to obtained the volume in cm^3. This is performed thanks to standard (metal) cylinders that are measured with the apparatus. Since their volume is known in advance (e.g. by manual or another procedure), a conversion pixel^3 to cm^3 is directly obtained. Better results are obtained if standards of similar size and surface reflective properties are used (to achieve this in our case, the metal standards were flat-black painted). For instance, for the 10 cm long specimens, 10 cm long standards were used, 15 cm for 15 cm long specimens, etc.

4. Results

Different tests were performed to assess the proposed procedure. For instance, Fig. 6 shows the variation of measurement for a given specimen measured consecutively five times. This allows in fact to assess the intrinsic error of the system. As seen, the error is larger on the length with respect to the diameter. In fact this is due to the limited number of measured lengths since due to the edge curvatures observed in Fig. 2-5, only a limited set of lengths are extracted per image. Fortunately, as seen in eq. 1, volume computation is more affected by errors on diameter than by error in length.

Table 1: Comparison between manual and vision measurement approaches for 3 sample lengths

	manual	**vison**	**manual**	**vison**	**manual**	**vison**
***L* (cm)**	**5**	**5**	**10**	**10**	**15**	**15**
d*L*(cm)	**0.005**	**0.025**	**0.005**	**0.02**	**0.005**	**0.05**
***D* (cm)**	**5**	**5**	**5**	**5**	**5**	**5**
d*D* (cm)	**0.005**	**0.005**	**0.005**	**0.005**	**0.005**	**0.005**
***V* (cm^3)**	**98.17477188**	**98.174772**	**196.3495438**	**196.34954**	**294.5243156**	**294.52432**
d*V*(cm^3)	**0.294524316**	**0.6872234**	**0.490873859**	**0.7853982**	**0.687223403**	**1.5707964**

The procedure was tested on thirty samples that were previously manually measured. Table 1 summarizes the results. Overall, it is seen that, with the current experimental set-up, the diameter measurement errors are similar for both approaches while the length measurement errors are as much as ten times worse in the case of the vision approach due to limited measurements in length (because of the perspective distortion as discussed previously). Fortunately, the length is less critical as explained and thus the overall volume errors for both methods are in the same range.

In the vision approach, the error is limited by the pixel size (+/- 1 pixel) corresponding to about 0.3 mm with the present set-up. However, better figures are achieved thanks to appropriate processing such as averaging (especially in the case of diameters).

5. Conclusion

In this paper a vision approach for cylindrical-shaped objects was presented and compared with the traditional manual measurement approach. While the goal of 0.1 cm^3 accuracy was not achieved with the experimental set-up made up from of-the-shelves equipment, a careful analysis of the error sources allow for the following recommendations that would permit to achieve the goal: add a laser line to illuminate the sample length and thus improve this measurement, proceed with a sub-pixel processing in the image segmentation, replace de Sobel operator with an enhanced Canny operator /1/, use of a 768 x 494 camera and optionally add 1 x 4096 line scan camera for the length measurement.

6. Acknowledgements

Help of Mr. Y. Chalifour and F. Galmiche of the EE Dept. (Université Laval) is appreciated.

References

/1/ D.H. Ballard, C.M. Brown, Computer Vision, Prentice-Hall (1982), 523 p.

/2/ G. Deltel *et al.*, *Système de mesure de la densité d'échantillons*, Vision Laboratory, EE Dept., Université Laval (May 2001) 69 p. [in French]

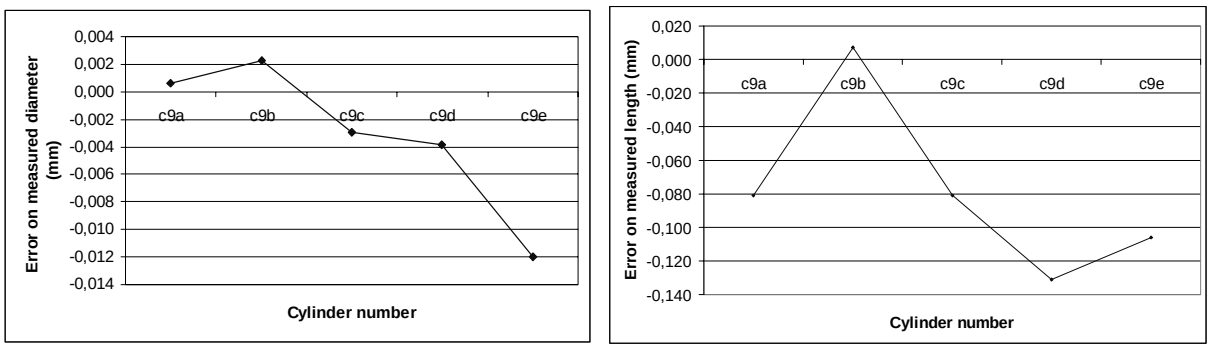

Fig.6: Consecutive measurement errors.

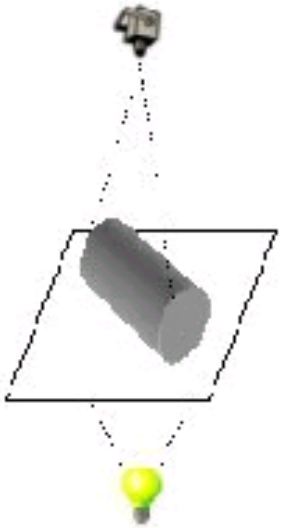

measurement principle

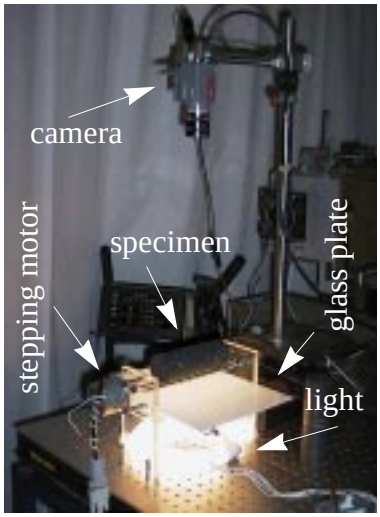

picture of the experimental set-up

[side view: short side] *[side view: long side]*

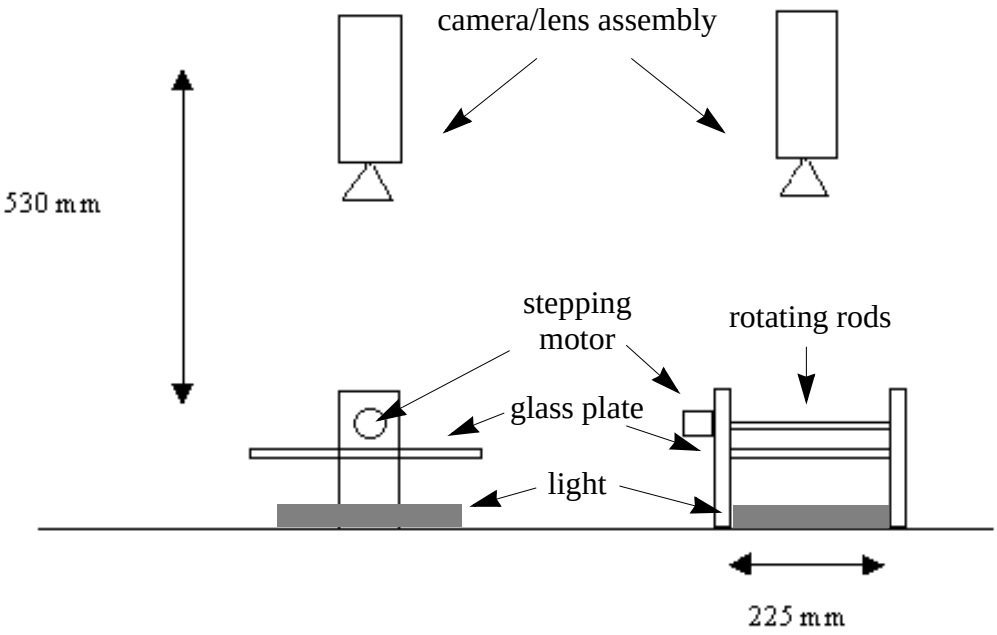

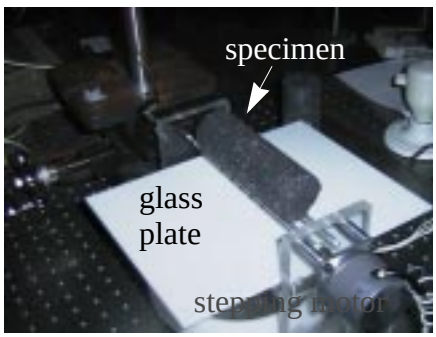

picture of the experimental set-up

Fig. 1: Experimental set-up: schematic diagrams and and pictures.

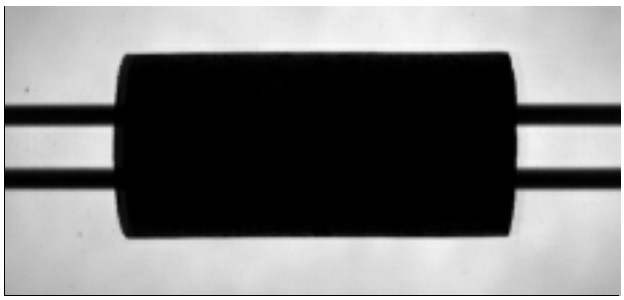

Fig. 2: Original gray level image (256 gray levels).

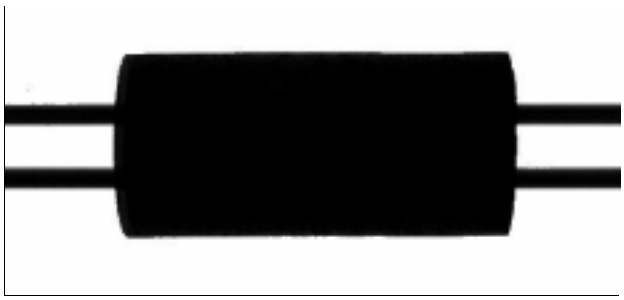

Fig. 3: First binarization, image of Fig. 2.

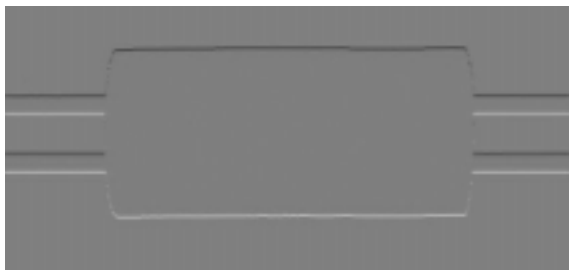

Fig. 4: Convolution of image of Fig. 3 with the Sobel operator: [-1 0 1, -2 0 2, -1 0 1].

Fig. 5: Maximum and minimum per colomn for image of Fig. 4.